Particularities of mathematical modeling of deformation processes for arched and panel designs of composites with large displacements and rotation angles

Vladimir G. DMITRIEV*,[1], Olga V. EGOROVA[2], Eduard I. STAROVOITOV[3]

*Corresponding author
[1]Institute of Aerospace,
Moscow Aviation Institute (National Research University),
4 Volokolamskoe Shosse, 125993, Moscow, Russian Federation,
vgd2105@mail.ru*
[2]Department of Resistance of Materials Dynamics and Strength of Machines,
Moscow Aviation Institute (National Research University),
4 Volokolamskoe Shosse, 125993, Moscow, Russian Federation,
janus_olga@mail.ru
[3]Department of Building Mechanics,
Belarusian State University of Transport,
34 Kirov Str., 246653, Gomel, Republic of Belarus,
edstar0@yandex.by

DOI: 10.13111/2066-8201.2020.12.S.5

Received: 13 March 2020/ Accepted: 27 May 2020/ Published: July 2020

Abstract: *In aerospace systems and automotive industry flexible elastic and thin-walled structures are widely used. The adequate mathematical models are in the process of development as well as numerical algorithms for examination of the features of processes of deformation of panel and arch designs with large displacements and arbitrary angles of rotation of the normal. For the discretization of the original continuum problem in spatial variables, the finite difference method can be used with the replacement of differential operators by finite-difference second-order approximations. The computational algorithm for solving a substantially nonlinear boundary-value problem is constructed on the basis of adaptation of the calculation method with construction of an explicit two-layer difference scheme in time of the second order of accuracy. The influence of the boundary conditions on the features of subcritical and supercritical behavior of the elastic arch structure under the influence of the surface load of the "tracking" type is considered.*

Key Words: *finite differences, nonlinear problems, linear iterative process, method of establishment, boundary conditions*

1. INTRODUCTION

Flexible elastic thin-walled structures are widely used in various fields of modern technology, in particular in aerospace systems [1], [2], [3], [4] (including expandable antennas, protective shields [5], [6], [7], [8]), and in automotive industry (car springs made of multilayer composites, pneumatic tires of a diagonal structure [9])), etc. The influence of the boundary conditions on the features of the subcritical and supercritical behavior of the elastic arch

structure under the influence of the surface load of the "tracking" type is considered. In deriving the initial geometric and physical relations, traditional assumptions of the beam theory are used: the hypothesis of flat sections and the hypothesis of the absence of normal stresses in longitudinal sections. The median surface of the arch (panel) is taken as the coordinate surface (cast surface) of the single-layer structure, and for the multilayer structure, the median surface of one of the layers, the contact surface of the layers, or the line passing through the centers of gravity of cross sections can be assumed. The cross-sectional dimension normal to the axis in the plane of the rod is assumed to be small compared to the radius of curvature of deformed axis. To describe the processes of deformation of elastic arches (panels) with large displacements of the points of coordinate surface and unlimited angles of rotation of the normal to it, the Cartesian coordinates *x*, *y* can be accepted as unknowns, since the use of traditional components of tangential u and normal w displacement for the considered version of geometrically nonlinear deformation of thin-walled constructions leads to significant complication of the structure of equations [10], [11].

2. THE MATHEMATICAL MODEL OF DEFORMATION OF SINGLE-LAYER AND MULTI-LAYER ARCH STRUCTURES

Prior to deformation, an element with undeformed generatrix length ds_0 has initial coordinates x_0, y_0, curvature k_{10} and an initial angle θ_0 between the x axis and the normal to the generator (Figure 1). Putting the coordinates x_0, y_0 with the given functions of linear coordinate along the generatrix $x_0 = x_0(s_0)$, $y_0 = y_0(s_0)$, for the initial (undeformed) state, we can write the following

$$ds_0 = \sqrt{dx_0^2 + dy_0^2} \tag{1}$$

$$\sin\theta_0 = \frac{dx_0}{ds_0} \tag{2}$$

$$\cos\theta_0 = \frac{dy_0}{ds_0} \tag{3}$$

$$ds_0 = R_{10} \cdot d\theta_0 \tag{4}$$

$$k_{10} = \frac{1}{R_{10}} = \frac{d\theta_0}{ds_0} \tag{5}$$

where R_{10} is the radius of curvature in direction of the generatrix (Figure 1).

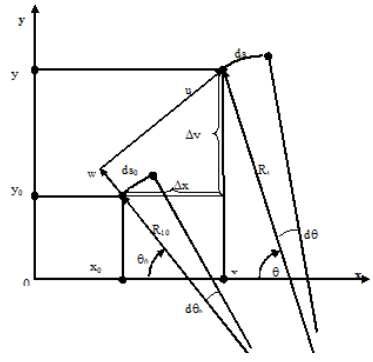

Fig. 1 - Deformation kinematics

As a result of deformation, the element will have the length ds, x, y coordinates, a rotation angle θ, and curvatures k_1. Considering the coordinates x, y as a function of the linear coordinate s along the deformed generatrix $x = x(s)$, $y = y(s)$, for the deformed state we have relations similar to (1-5).

$$ds = \sqrt{dx^2 + dy^2} \tag{6}$$

$$\sin\theta = \frac{dx}{ds} \tag{7}$$

$$\cos\theta = \frac{dy}{ds} \tag{8}$$

$$ds = R_1 \cdot d\theta \tag{9}$$

$$k_1 = \frac{1}{R_1} = \frac{d\theta}{ds} \tag{10}$$

where θ is the angle of rotation similar to kinematic parameter of the "rigid" normal in the framework of Kirchhoff – Love hypotheses. Furthermore, for the mathematical model under consideration, restrictions on rotation angles θ are not imposed. The components of the deformation along the generatrix E_{11}, as well as the change in curvature of the surface of the cast K_{11} are defined as

$$E_{11} = \frac{ds - ds_0}{ds_0} = \frac{ds}{ds_0} - 1 \tag{11}$$

$$K_{11} = k_1 - k_{10} = \frac{d\theta}{ds} - \frac{d\theta_0}{ds_0} \tag{12}$$

Strain components for fiber of arch (panel) at distance z from the surface coordinate with the accepted assumptions and hypotheses $z,\cdot k_{10} < 1$ are distributed linearly

$$E_{11}^z = E_{11} + z \cdot K_{11} \tag{13}$$

Let us introduce the force factors in the cross section of the arch: the longitudinal T, the transverse force Q and the bending moment M, as well as $q_u = q_u(s)$ and $q_w = q_w(s)$ – the components of intensity of distributed load $q = q(s)$ on kernel. For the case of single-layer structure made of material with Young E modulus and Poisson's ratio v we have

$$T = B_{11}E_{11} \tag{14}$$

$$M = D_{11}K_{11} \tag{15}$$

where for arched construction:

$$B_{11} = E \cdot F \tag{16}$$

$$D_{11} = E \cdot J \tag{17}$$

and where for the elastic panels with their cylindrical bending:

$$B_{11} = \frac{E \cdot h}{1 - v^2} \tag{18}$$

$$D_{11} = \frac{E \cdot h^3}{12 \cdot (1 - v^2)} \tag{19}$$

In (16-19) F and J are the area and moment of inertia of cross-sectional arch relative its main central axis, h is the thickness of the panel.

For multilayer structure as a whole, the conditions of hard contact of the layers without reciprocated separation and slipping are accepted, while in general case, layers of variable thickness h_m are considered; m is the layer index: $1 \leq m \leq M$, M is the number of layers (Figure 2).

Force factors in multilayer element are expressed through the components of deformation of the coordinate surface according to the formulas [11].

$$T = B_{11}E_{11} + A_{11}K_{11} \tag{20}$$

$$M = A_{11}E_{11} + D_{11}K_{11} \tag{21}$$

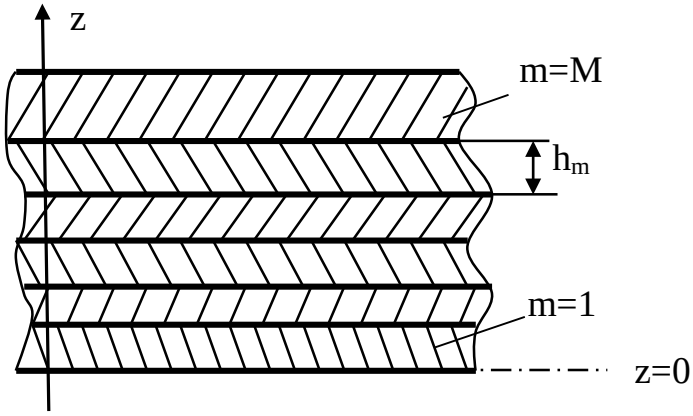

Fig. 2 - The Composition Package Structure

The stiffness coefficients A_{11}, B_{11}, D_{11} in formulas (20, 21) are determined through the elastic characteristics of layers and their thickness as:

–for the arched construction:

$$B_{11} = \sum_{m=l_z}^{M} \int_{m-1}^{z_m} b \cdot E_m dz \tag{22}$$

$$A_{11} = \sum_{m=1}^{M} \int_{z_{m-1}}^{z_m} b \cdot E_m z dz \tag{23}$$

$$D_{11} = \sum_{m=1}^{M} \int_{z_{m-1}}^{z_m} b \cdot E_m z^2 dz \tag{24}$$

–for the panel structure:

$$B_{11} = \sum_{m=1}^{M} \int_{z_{m-1}}^{z_m} \frac{E_m}{1 - v_m^2} dz \tag{25}$$

$$A_{11} = \sum_{m=1}^{M} \int_{z_{m-1}}^{z_m} \frac{E_m \cdot z}{1 - v_m^2} dz \tag{26}$$

$$D_{11} = \sum_{m=1}^{M} \int_{z_{m-1}}^{z_m} \frac{E_m \cdot z^2}{1 - v_m^2} dz \tag{27}$$

where $b = b(z)$ is width of the arch (in particular case $b = const$), E_m, v_m are Young's moduli and Poisson's ratios of m^{th} layer. Assuming that the physical and mechanical characteristics of the material of m^{th} layer are constant within the layer and counting z coordinate from the lower (free) surface of the first layer of the panel surface ($m = 1$, Figure 2), formulas (22-27) can be reduced to:

– for arched construction:

$$B_{11} = \sum_{m=1}^{M} b \cdot E_m \cdot (z_m - z_{m-1}) \tag{28}$$

$$A_{11} = \frac{1}{2} \sum_{m=1}^{M} b \cdot E_m \cdot (z_m^2 - z_{m-1}^2) \tag{29}$$

$$D_{11} = \frac{1}{3} \sum_{m=1}^{M} b \cdot E_m \cdot (z_m^3 - z_{m-1}^3) \tag{30}$$

– for panel constructions:

$$B_{11} = \sum_{m=1}^{M} \frac{E_m \cdot (z_m - z_{m-1})}{1 - v_m^2} \tag{31}$$

$$A_{11} = \frac{1}{2} \sum_{m=1}^{M} \frac{E_m \cdot (z_m^2 - z_{m-1}^2)}{1 - v_m^2} \tag{32}$$

$$D_{11} = \frac{1}{3} \sum_{m=1}^{M} \frac{E_m \cdot (z_m^3 - z_{m-1}^3)}{1 - v_m^2} \tag{33}$$

The equations of equilibrium of an arch element (panel) in the projections on the axis, associated with the deformed coordinate surface, have this form

$$\frac{dT}{ds} + k_1 Q + q_u = 0 \tag{34}$$

$$\frac{dQ}{ds} - k_1 T + q_w = 0 \tag{35}$$

$$Q = \frac{dM}{ds} \tag{36}$$

Equations (1-36) are supplemented by boundary conditions at the edges of $s = s_0$ and $s = s_L$.

Let us formulate the most important boundary conditions in practical terms at the edge $s = s_0$ (Figure 3):

–hard pinching (Figure 3a)

$$x(s_0) = x_0 \tag{37}$$

$$y(s_0) = y_0 \tag{38}$$

$$\theta(s_0) = \theta_0 \tag{39}$$

–hinging (Figure 3b):

$$x(s_0) = x_0 \tag{40}$$

$$y(s_0) = y_0 \tag{41}$$

$$k_1(s_0) = k_0 = 1/R_{10} \tag{42}$$

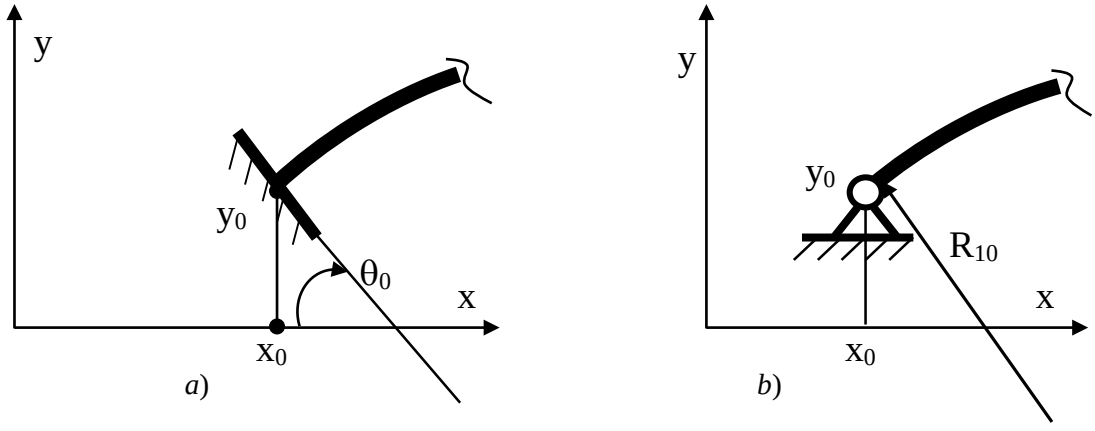

Fig. 3 - Boundary conditions

The boundary conditions at boundary $s = s_L$ are formulated similarly to (37-42).

3. COMPUTATIONAL ALGORITHM OF NONLINEAR DIFFERENTIAL EQUATIONS

In the numerical solution of system of nonlinear differential equations (1-42), spatial discretization can be performed by the finite difference method (FDM) [12], [13]. In the area of continuous variation of argument s_0 (s stands for deformed state) two grids are introduced: the main one with integer indices i and the auxiliary one with indices $i \pm 1/2$, the nodes of which are located in the middle between the nodes of the main mesh $i \pm 1$ (Figure 4). To increase the precision and convergence of the difference scheme, the parameters of stress-strain state (SSS) (1-13) are related to the nodes of both the main and auxiliary grids. Partial derivatives are approximated by difference operators of the second order of precision. The initial geometry can be defined by the grid functions $(x_0)_i$, $(y_0)_i$. Then the finite-difference approximations of differential relations (1-12) for the initial state can be represented as follows (Figure 4)

$$(\Delta s_0)_{i-1/2} = \Delta s_1 = \sqrt{\Delta x_1^2 + \Delta y_1^2} \tag{43}$$

$$(\Delta s_0)_{i+1/2} = \Delta s_2 = \sqrt{\Delta x_2^2 + \Delta y_2^2} \tag{44}$$

$$\sin\alpha_1 = \frac{\Delta y_1}{\Delta s_1} \tag{45}$$

$$\theta_1 = (\theta_0)_{1-1/2} = \frac{\pi}{2} - \alpha_1 \tag{46}$$

$$\sin\alpha_2 = \frac{\Delta y_2}{\Delta s_2} \tag{47}$$

$$\theta_2 = (\theta_0)_{1+1/2} = \frac{\pi}{2} - \alpha_2 \tag{48}$$

$$(\Delta s_0)_i = \frac{(\Delta s_0)_{i-1/2} + (\Delta s_0)_{i+1/2}}{2} \tag{49}$$

$$(k_{10})_i = \frac{(\theta_0)_{i+1/2} - (\theta_0)_{i-1/2}}{(\Delta s_0)_i} \tag{50}$$

where

$$\Delta x_1 = (x_0)_i - (x_0)_{i-1} \tag{51}$$

$$\Delta y_1 = (y_0)_i - (y_0)_{i-1} \tag{52}$$

$$\Delta x_2 = (x_0)_{i+1} - (x_0)_i \tag{53}$$

$$\Delta y_2 = (y_0)_{i+1} - (y_0)_i \tag{54}$$

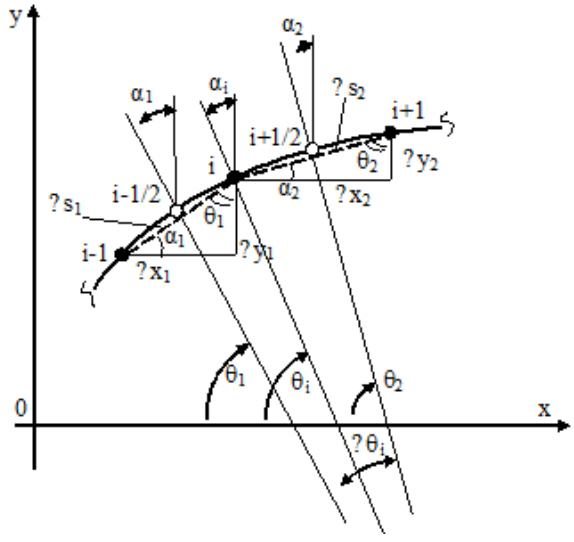

Fig. 4 - Finite-difference approximations of the differential relations (1) for the initial state

In relations (43-54), grid functions $(x_0)_i$, $(y_0)_i$ are set from the condition that the step is constant $\Delta s_0 = const$ for entire computational domain $0 \le s_0 \le L_0$, so that

$$\Delta s_0 = \frac{L_0}{N-1} \tag{55}$$

$$\Delta s = (\Delta s_0)_{i-1/2} = (\Delta s_0)_{i+1/2} \tag{56}$$

where N is number of sampling points: $1 \le i \le N$.

The deformed state can be described by grid nodal displacement functions x_i and y_i the approximation of equations (6-10) by finite-difference operators, similar to (43-54) (Figure 4).

$$\Delta s_{i-1/2} = \Delta s_1 = \sqrt{\Delta x_1^2 + \Delta y_1^2} \tag{57}$$

$$\Delta s_{i+1/2} = \Delta s_2 = \sqrt{\Delta x_2^2 + \Delta y_2^2} \tag{58}$$

$$\sin\alpha_1 = \frac{\Delta y_1}{\Delta s_1} \tag{59}$$

$$\sin\alpha_2 = \frac{\Delta y_2}{\Delta s_2} \tag{60}$$

$$\theta_1 = \theta_{i-1/2} = \frac{\pi}{2} - \alpha_1 \tag{61}$$

$$\theta_2 = \theta_{i+1/2} = \frac{\pi}{2} - \alpha_2 \tag{62}$$

$$\Delta s_i = \frac{\Delta s_{i-1/2} + \Delta s_{i+1/2}}{2} \tag{63}$$

$$(k_1)_i = \frac{\theta_{i+1/2} - \theta_{i-1/2}}{\Delta s_i} \tag{64}$$

where

$$\Delta x_i = x_i - x_{i-1} \tag{65}$$

$$\Delta y_i = y_i - y_{i-1} \tag{66}$$

$$\Delta x_2 = x_{i+1} - x_i \tag{67}$$

$$\Delta y_2 = y_{i+1} - y_i \tag{68}$$

The grid functions of deformation component E_{11} in (11, 12) are related to the nodes of the auxiliary grid $i \pm 1/2$, and the grid functions of curvature change K_{11}; they are approximated at the nodes of the main grid i

$$(E_{11})_{i-1/2} = \frac{\Delta s_{i-1/2} - (\Delta s_0)_{i-1/2}}{(\Delta s_0)_{i-1/2}} \tag{69}$$

$$(E_{11})_{i+1/2} = \frac{\Delta s_{i+1/2} - (\Delta s_0)_{i+1/2}}{(\Delta s_0)_{i+1/2}} \tag{70}$$

$$(K_{11})_i = (k_1)_i - (k_{10})_i \tag{71}$$

It is easy to see that the same-type finite-difference approximations (16-19) and (43-54) are used to describe both initial and deformed states. When approximating the physical relations (20-36) in accordance with (69-71), the mesh functions for longitudinal T and transverse Q forces are determined at the nodes of auxiliary mesh $i \pm 1/2$, and the mesh

functions of the bending moment M are approximated at nodes of the main mesh i. The finite-difference analogues of the equilibrium equations (34-36), discretized with respect to the nodal point of the main grid i, can be written in this form

$$\frac{\mathrm{T_{i+1/2}} - \mathrm{T_{i-1/2}}}{\Delta s} + 0.5 \cdot (\mathrm{k_1})_\mathrm{i} \cdot (\mathrm{Q_{i-1/2}} + \mathrm{Q_{i+1/2}}) + (\mathrm{q_u})_\mathrm{i} = 0 \tag{72}$$

$$\frac{\mathrm{Q_{i+1/2}} - \mathrm{Q_{i-1/2}}}{\Delta s} + 0.5 \cdot (\mathrm{k_1})_\mathrm{i} \cdot (\mathrm{T_{i-1/2}} + \mathrm{T_{i+1/2}}) + (\mathrm{q_w})_\mathrm{i} = 0 \tag{73}$$

$$\mathrm{Q_{i+1/2}} = \frac{M_i - M_{i-1}}{\Delta s_1} \tag{74}$$

$$\mathrm{Q_{i+1/2}} = \frac{M_{i+1} - M_i}{\Delta s_2} \tag{75}$$

where $(\mathrm{q_u})_\mathrm{i}$, $(\mathrm{q_w})_\mathrm{i}$ are the grid functions of the surface load components. Since the same finite-difference approximations (44-50) and (51-54) are used to approximate the SSS parameters in both the initial and deformed states, at $(\mathrm{q_u})_\mathrm{i} = (\mathrm{q_w})_\mathrm{i} = 0$ the undeformed state defined by relations (44-50) is an exact solution of the grid equations (72), which confirms the correctness of the established difference approximations (43-70). For the numerical solutions of the system of difference equations (72) using a quasi-dynamic shape method and establishing transition to evolution problem by substituting equations (22) for equation coinciding in shape with the equations of motion of the shell in viscous medium [12], [13], [14], [15], [16]. For the case of "tracking" load, to simplify the computational procedure, it is advisable to make an iterative process with respect to displacements of the local basis u, w with subsequent recalculation in the x, y coordinate system (Figure 1). We denote the finite-difference analogues of the equilibrium equations (72) in operator form as

$$[L_{\Delta s}(U_k)]_i + (q_k)_i = 0 \tag{76}$$

where $[L_{\Delta s}(U_k)]_i$ are corresponding generalized finite-difference operators for the vector U_k of mesh displacement functions: $U_1 = u_1$, $U_2 = w_i$, $(q_1)_i = +(q_u)_i$, $(q_2)_i = +(q_w)_i$; $(k = 1{,}2)$. Then the non-stationary equations of the establishment method can be written as follows

$$[L_{\Delta s}(U_k)]_i + (q_k)_i \tag{77}$$

where εk are specific viscosity parameters of the medium, ρ is the density, $m_k = \rho h$ $(k = 1{,}2)$. The point indicates the differentiation with respect to time t. The approximation of equations (25) on time grid with step $\Delta t = const$ using difference operators of second-order of precision $O(\Delta t^2)$ allows us to explicitly express the velocities on the time layer $t(n + 1/2)$ and grid functions of generalized displacements on the time layer $t(n + 1)$.

$$[\dot{u}_k]_i^{(n+1/2)} = \frac{[2m_k - \varepsilon_k \Delta t]_i}{[2m_k + \varepsilon_k \Delta t]_i} \cdot [\dot{u}_k]_i^{(n-1/2)} + \frac{2\Delta t \cdot [L_{\Delta s}(U_k) + q_k]_i^{(n)}}{[2m_k + \varepsilon_k \Delta t]_i} \tag{78}$$

$$[u_k]_i^{(n+1)} = [u_k]_i^{(n)} + \Delta t \cdot [\dot{u}_k]_i^{(n+1/2)} \tag{79}$$

Grid functions of displacement of nodal points x_i, y_i in the coordinate system x, y are defined through the grid functions of displacement of components u_i, w_i using the formulas of transition

$$x_1 = (x_0)_i + \Delta x_i \tag{80}$$

$$y_1 = (y_0)_i + \Delta y_i \tag{81}$$

Where (Figure 1)

$$\Delta x_1 = u_1 \cdot \sin(\theta_0)_i - w_i \cdot \cos(\theta_0)_i \tag{82}$$

$$\Delta y_1 = u_1 \cdot \cos(\theta_0)_i - w_i \cdot \sin(\theta_0)_i \tag{83}$$

Hence, the difference approximation of non-stationary equations (77) leads to iterative process (26) of finding a solution to the original stationary problem (76). The parameters of the iterative process – the specific viscosities of the medium $\varepsilon_k(i)$ and the time step Δt - are determined from the conditions for accelerating the convergence and stability of the difference scheme [12].

For the case of stationary iterative process, the estimation formulas taking into account the structure of equations (77) can be written in the form [13], [14], [15], [16].

$$\varepsilon_k = 2a_{\varepsilon,(k)}\sqrt{\frac{m_k\mu_{1,(k)}\mu_{2,(k)}}{\mu_{1,(k)} + \mu_{2,(k)}}} \tag{84}$$

$$\Delta \mathrm{t_k} = 2\alpha_{\mathrm{t,(k)}}\sqrt{\frac{m_k}{\mu_{1,(k)} + \mu_{2,(k)}}} \tag{85}$$

where $\mu_{1,(k)}$ and $\mu_{2,(k)}$ are the smallest and largest eigenvalues for the corresponding difference operators in equations (25); $a_{\varepsilon,(k)}$ and $a_{t,(k)}$ are correction factors close to 1. The time step $\Delta \mathrm{t}$ for the entire difference scheme is determined from the condition of form: For nonlinear problems, the exact determination of the boundaries of spectra of difference operators is associated with significant mathematical difficulties, therefore, $\mu_{1,(k)}$ and $\mu_{2,(k)}$ are estimated in the framework of linear relations for simplifications in the original equations. The evaluation formulas for $\mu_{1,(k)}$ and $\mu_{2,(k)}$ for the case of a single-layer orthotropic structure described by physical relations (14-19) can be represented as follows:

–the smallest eigenvalues

$$\mu_{1,(1)} = 4\frac{B_{11}}{\Delta s_0^2} \cdot sin^2\frac{\pi}{2}\frac{\Delta s_0}{L_0} \tag{86}$$

$$\mu_{1,(2)} = 16\frac{D_{11}}{\Delta s_0^4} \cdot sin^4\frac{\pi}{2}\frac{\Delta s_0}{L_0} + k_{10}^2 B_{11} \tag{87}$$

–the largest eigenvalues

$$\mu_{2,(1)} = 4\frac{B_{11}}{\Delta s_0^2} \cdot cos^2\frac{\pi}{2}\frac{\Delta s_0}{L_0} \tag{88}$$

$$\mu_{2,(2)} = 16\frac{D_{11}}{\Delta s_0^4} \cdot cos^4\frac{\pi}{2}\frac{\Delta s_0}{L_0} + k_{10}^2 B_{11} \tag{89}$$

where k_{10} is the characteristic of curvatures. During calculation of real structures ratio/is usually large, and therefore (establishing method constructed in the form of optimal linear iterative process 26), reduces the number of iterations around time as compared with using the method of establishing when the right sides of equations (77) cover only the second term [12], [13], [17].

4. NUMERICAL RESULTS OF STUDYING NONLINEAR DEFORMATION OF ELASTIC ARCH STRUCTURE

Based on the developed mathematical models and computational algorithms, studies were performed on the features of nonlinear deformation of elastic arch structure under various options of boundary conditions. A single-layer arched structure of constant thickness h was considered under the action of static uniformly distributed external load of "tracking" type with intensity q_w. The undeformed (initial) contour of the arch is part of the circular arc with an initial radius of curvature R_{10} (Figure 5). Geometric parameters of the arch: $R_{10}/h = 200$; $\theta_0 = 15°$; $\theta_L = 75°$. The cross section of the arch is rectangle of width b and height h with aspect ratio: $b/h = 4$.

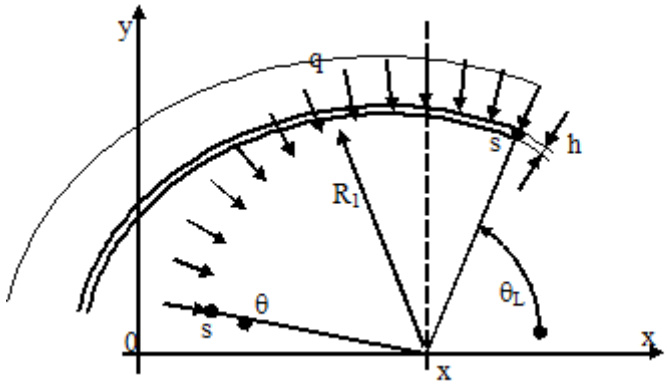

Fig. 5 - Undeformed (initial) contour of the arch

In numerical solution of the problem, the number of sampling points was taken equal to $N = 47$. The studies have demonstrated that formulas (84-89) allow us to obtain fairly accurate (from the point of view of convergence and stability) estimates of the values of iterative parameters. Thus, for example, in both the subcritical and essentially nonlinear supercritical regions of deformation, the stability of iterative process (77-79) was ensured for the time step Δt calculated in accordance with (29) with the correction coefficient $\alpha_{t,(k)} = 0.8$. The intensity of the external pressure q_w distributed along the entire span of the arch was determined through the value of load parameter p_q with respect to the critical pressure q_{cr} for circular ring with radius $R = R_{10}$

$$q_w = p_q \cdot q_{cr} \tag{90}$$

$$q_{cr} = \frac{3 \cdot D_{11}}{R^3} \tag{91}$$

Three variants of relating the boundary conditions at the edges $s = s_0$ and $s = s_L$ were considered:

– variant $C - C$: the edges $s = s_0$ and $s = s_L$ are clamped – the boundary conditions (37);

– variant $C - H$: the edges $s = s_0$ and $s = s_L$ are hinged – boundary conditions (41);

– variant $C - H$: the edge $s = s_0$ is clamped, and the edge of $s = s_L$ is hinged.

The results of the computational experiment are presented in Figures 6-9. Figure 6 shows waveforms of arches deformed surface after buckling to variant $C - C$, where 2,3,4 curves correspond to $p_q = 11.43; 22.86; 137.14$, and in Figure 7 for the $C - H$ variant, curves 2, 3 correspond to $p_q = 7.3; 7.86$. Curve 1 in Figures 6, 7 is the initial (undeformed) shape of the

arch. Figure 8 shows the variation of the curvatures of k_1/k_{10}, and Figure 9 – shows change in the normal rotation angles $\Delta\theta = \theta - \theta_0$, where curves 1 correspond to the variant of boundary conditions $C - C$ in $p_q = 137.14$, and curves 2 correspond to the variant $C - H$ at $p_q = 7.86$. Line 3 in Figure 8 corresponds to the initial curvature of the arch $k_{10} = const$.

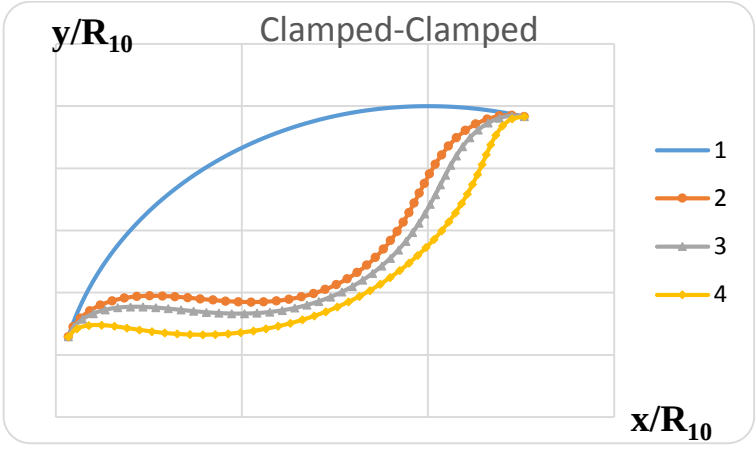

Fig. 6 - Shape of the deformed surface of the arch after loss of stability for variant $C - C$

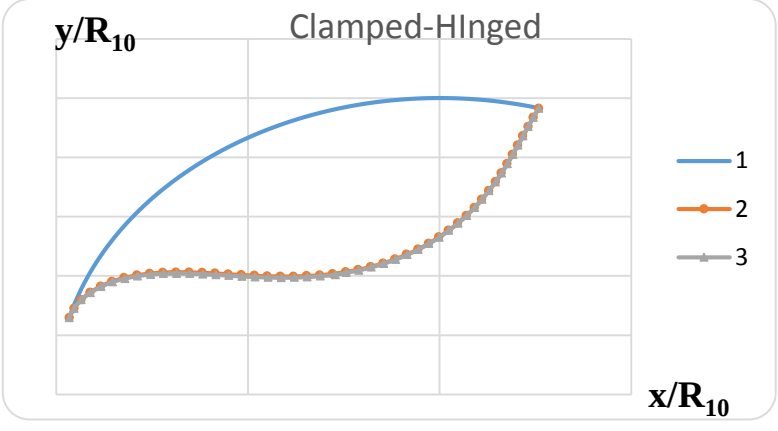

Fig. 7 - Shape of the deformed surface of the arch after loss of stability for variant $C - H$

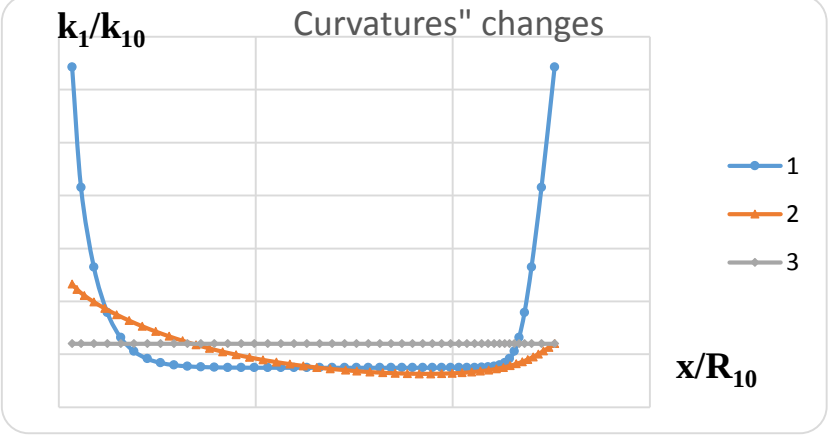

Fig. 8 - The change in curvature k_1/k_{10}

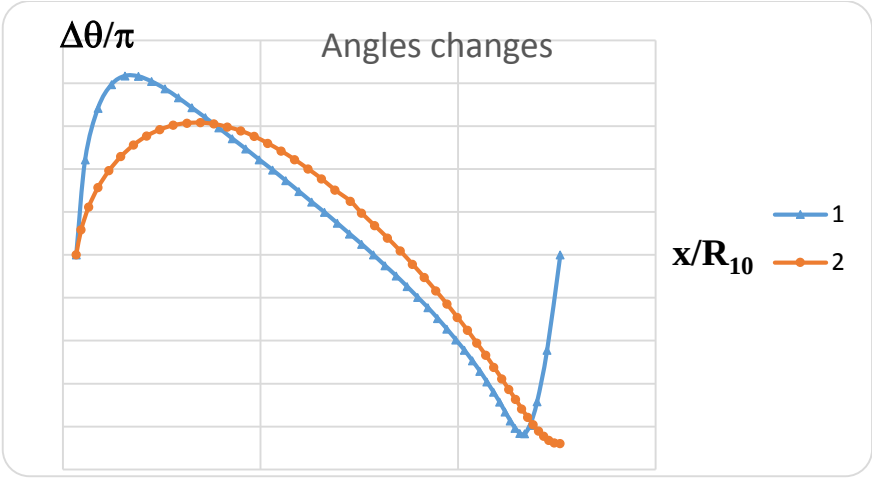

Fig. 9 - Changes in the rotation angles of the normal $\Delta\theta = \theta - \theta_0$

5. CONCLUSIONS

The results of the studies have demonstrated that the boundary conditions significantly affect the nature of deformation of flexible arch in both the subcritical and supercritical areas. If for option $C - C$ after the initial loss of stability with significant geometry change at $p_q = 10.86$ arch continued to bear an increasing load until the occurrence and development of plastic deformations, then with hinged edges (option $H - H$) after loss of stability at $p_q = 5.08$, the absence of balanced forms with increasing load was manifested in divergence of iterative process.

For the variant $C - H$ after the initial loss of stability at $p_q = 7.28$, the arch accepted an increasing load up to a complete loss of stability at $p_q = 7.91$. The transition from the initial balanced shape of the arch, very close to the original, to the supercritical state occurred abruptly from the values of maximum displacements $\max(u, w) \approx 0.2\ h$ to values in the supercritical region of the order of $\max(u, w) \approx 110\ h$ and rotation angles of the normals $\max(\Delta\theta) \approx 0.5\ \pi$.

ACKNOWLEDGMENTS

The work has been conducted with the financial support of the grants of the Russian Foundation for Basic Research (RFBR grant No 19-01-00675).

REFERENCES

[1] M. Kuprikov and L. N. Rabinskiy, Vertical take-off and landing aircrafts: Myth or reality of modern aviation, *Journal of Mechanical Engineering Research and Developments*, vol. **41**, no. 4, pp. 46-52, 2018.

[2] M. Y. Kuprikov, N. M. Kuprikov and L. N. Rabinskiy, Business objective for the life cycle of aircraft, *INCAS Bulletin*, vol. **11**, Special Issue, pp. 163-174, 2019, https://doi.org/10.13111/2066-8201.2019.11.S.16.

[3] M. Kuprikov and L. N. Rabinskiy, Cross-polar routes as a factor that changed the geometric layout of long-haul aircrafts flying over long distances, *Journal of Mechanical Engineering Research and Developments*, vol. **41**, no. 4, pp. 53-57, 2018.

[4] M. Y. Kuprikov, N. M. Kuprikov and L. N. Rabinskiy, The dependence of the appearance of the aircraft on the conditions of the arctic basing, *INCAS Bulletin*, vol. **11**, Special Issue, pp. 115-123, https://doi.org/10.13111/2066-8201.2019.11.S.11, 2019.

[5] B. A. Antufev, O. V. Egorova, A. L. Medvedskii and L. N. Rabinskiy, Dynamics of shell with destructive heat-protective coating under running load, *INCAS Bulletin*, vol. **11**, Special Issue, pp. 7-16, 2019, https://doi.org/10.13111/2066-8201.2019.11.S.1.

[6] B. A. Antufev, O. V. Egorova and L. N. Rabinskiy, Quasi-static stability of a ribbed shell interacting with moving load, *INCAS Bulletin*, vol. **11**, Special Issue, pp. 33-39, 2019, https://doi.org/10.13111/2066-8201.2019.11.S.4.

[7] B. A. Antufev, O. V. Egorova and L. N. Rabinskiy, Dynamics of a cylindrical shell with a collapsing elastic base under the action of a pressure wave, *INCAS Bulletin*, vol. **11**, Special Issue, pp. 17-24, https://doi.org/10.13111/2066-8201.2019.11.S.2, 2019.

[8] A. G. Getmanov and L. N. Rabinskiy, Assessment of durability of coatings in difficult stress conditions, *Periodico Tche Quimica*, vol. **16**, no.33, pp. 490-497, 2019.

[9] A. A. Kireenkov, D. V. Nushtaev and S. I. Zhavoronok, A new approximate model of type accounting for both deformed state and dry friction forces in the contact spot on the background of the coupled model, *MATEC*, vol. **211**, article number 00803, 2018. DOI: 10.1051/matecconf/201821108003.

[10] E. I. Grigolyuk and V. I. Shalashilin, *Problems of nonlinear deformation: A method for continuing the soluteion with respect to a parameter in nonlinear problems in the mechanics of a solid deformable body*, Nauka, 1988

[11] V. G. Dmitriev, V. I. Biryukov, O. V. Egorova, S. I. Zhavoronok and L. N. Rabinskii, Nonlinear deforming of laminated composite shells of revolution under finite deflections and normal's rotation angles, *Russian Aeronautics*, vol. **60**, no. 2, pp. 169-176, 2017.

[12] N. S. Bakhvalov, N. P. Zhidkov and G. M. Kobelkov, *Numerical methods*, Fizmatlit. Laboratory of Basic Knowledge, 2001.

[13] V. Dmitriev, Applied mathematic technologies in nonlinear mechanics of thin-walled constructions, in M. Ram and S. B. Singh (Eds.), *Mathematics Applied to Engineering and Management Sciences* (pp. 71-116), CRC Press Taylor & Francis Group, 2019.

[14] V. G. Dmitriev and I. N. Preobrazhensky, Deformation of flexible shells with cutouts, *Proceedings of the USSR Academy of Sciences. Solid Mechanics*, no. 1, pp. 177-184, 1988.

[15] V. G. Dmitriev, O. V. Egorova and L. N. Rabinsky, Solution of nonlinear initial boundary-value problems of the mechanics of multiply connected composite material shells on the basis of conservative difference schemes, *Composites: Mechanics, Computations, Applications: An International Journal*, vol. **6**, no. 4, pp. 265-277, 2015.

[16] V. G. Dmitriev, O. V. Egorova, S. I. Zhavoronok and L. N. Rabinsky, Investigation of buckling behavior for thin-walled bearing aircraft structural elements with cutouts by means of numerical simulation, *Russian Aeronautics*, vol. **61**, no. 2, pp. 165-174, 2018.

[17] E. L. Kuznetsova and L. N. Rabinskiy, Heat transfer in nonlinear anisotropic growing bodies based on analytical solution, *Asia Life Sciences*, no. 2, pp. 837-846, 2019.